General Formula for the Green's Function Approach to the Spin-1/2 Antiferromagnetic Heisenberg Model

Daiki Sasamoto* and Takao Morinari[†]
Course of Studies on Materials Science, Graduate School of Human
and Environmental Studies, Kyoto University, Kyoto 606-8501, Japan
(Dated: December 29, 2023)

A wide range of analytical and numerical methods are available to study quantum spin systems. However, the complexity of spin correlations and interactions limits their applicability to specific temperature ranges. The analytical approach utilizing Green's function has proved advantageous, as it allows for formulation without restrictions on the presence of long-range order and facilitates estimation of the spin excitation spectrum and thermodynamic quantities across the entire temperature range. In this work, we present a generalized formulation of the Green's function method that can be applied to diverse spin systems. The notable aspect of our approach is that the theory aligns with the high-temperature expansion results in the high-temperature regime. When the spatial dimension d is d > 3, our formulation effectively describes the magnetic long-range order as Bose-Einstein condensation occurring at the wave vector characteristic of the magnetic long-range order. As an application to a frustrated spin system, we consider the J_1 - J_2 model on the square lattice, incorporating nematic correlations. While our approach may not be robust enough to determine the ground state properties, it is capable of describing short-range correlations at finite temperatures to a certain extent. In the presence of strong frustration, accurate numerical calculations become essential. Within this framework, we compute the specific heat, the spin susceptibility, and the spin-wave gaps at characteristic wave vectors, and discuss the effects of frustration. Our primary focus here is on the spin one-half antiferromagnetic Heisenberg model on an arbitrary lattice. However, the Green's function approach can be extended to include other types of interactions and accommodate higher spin values.

I. INTRODUCTION

Quantum antiferromagnetic Heisenberg models are of utmost importance in exploring intriguing phenomena. Of particular significance is the case of spin-1/2, where quantum correlation effects are most pronounced. A well-known example is cuprate superconductors[1], where high-temperature superconductivity emerges upon hole doping in the quasi-two-dimensional spin-1/2 Heisenberg antiferromagnet. The rich physics of cuprate superconductors is likely linked to the phenomenon of quantum spin liquid. Originating from Anderson's proposal of the resonating valence bond state[2], extensive theoretical and experimental research has been devoted to spin liquid states[3–5], which may host exotic quantum states.

The exploration of novel quantum ground states poses a challenge due to their absence of long-range order. In cases where magnetic long-range order exists, mean-field theory can be applied, and quantum fluctuations around it can be considered. However, our particular interest lies in states lacking long-range order and exhibiting high entanglement. Analytically investigating such systems is a formidable task, necessitating the adoption of sophisticated numerical algorithms, such as the density-matrix renormalization group, tensor network algorithms, and others.

Our interest in quantum spin liquid states extends

beyond their ground states. We must also explore their finite-temperature properties, especially when considering high-temperature superconductivity and practical quantum devices. At finite temperatures, quantum Monte Carlo serves as a powerful numerical algorithm. However, it may encounter challenges, particularly in cases involving frustration, where the negative sign problem can arise.

In this paper, we employ a double-time Green's function method[6, 7]. This approach does not rely on longrange order and can be applied to finite-temperature properties. By employing a decoupling scheme in the equations of motion that preserves the spin rotational symmetry [8], we derive a general formula independent of spatial dimensionality and the range of the exchange interaction. The notable aspect of our approach is that the theory aligns with the high-temperature expansion results in the high-temperature regime. When the spatial dimension d is $d \geq 3$, our formulation effectively describes the magnetic long-range order as Bose-Einstein condensation occurring at the wave vector characteristic of the magnetic long-range order. As an application to a frustrated spin system, we consider the J_1 - J_2 model on the square lattice, incorporating nematic correlations. We develop a self-contained formulation of the theory that does not require inputs from other methods. While our approach may not be sufficiently robust to determine the ground state properties, it is capable of describing short-range correlations at finite temperatures to a certain extent.

The rest of the paper is organized as follows. In Sec. II, we derive a general theoretical formula. For the case of

^{*} sasamoto.daiki.38n@st.kyoto-u.ac.jp

[†] morinari.takao.5s@kyoto-u.ac.jp

 $d \geq 3$, we present the self-consistent equations, including Bose-Einstein condensation, which can occur at the wave vector characteristic of the magnetic long-range order. In Sec. III, we apply this formula to the d-dimensional hypercubic lattice. We demonstrate that our theory is consistent with other theories obtained for d = 1, 2, 3at finite temperatures. In Sec. IV, we investigate the J_1 - J_2 model. We compute the correlation functions at zero temperature. Despite using only a single parameter for the decoupling approximation, our results are in good agreement with previous works employing several decoupling parameters. We also explore finite temperature properties to a certain extent. We compute the specific heat, the spin susceptibility, and the spin-wave gaps at characteristic wave vectors, and discuss the effects of frustration.

II. FORMULATION

We consider a general spin-1/2 quantum Heisenberg antiferromagnet on an arbitrary lattice, with the Hamiltonian expressed as:

$$H = \sum_{\langle i,j \rangle} J_{ij} \mathbf{S}_i \cdot \mathbf{S}_j, \tag{1}$$

where $S_i = (S_i^x, S_i^y, S_i^z)$ represents the spin-1/2 operator at site i. The parameter $J_{ij} = J_{ji}$ denotes the interaction strength between the spins at sites i and j, and $\langle i, j \rangle$ indicates the sum over a general pair of spins on the lattice.

In the double-time Green's function method, we study the equation of motion for the spin Green's function. To facilitate this analysis, we find it convenient to work with the Matsubara Green's function rather than the real-time Green's function. Denoting the imaginary time by τ and introducing the imaginary time ordering operator T_{τ} , the Matsubara Green's function is defined as follows:

$$\mathcal{G}_j(\tau) = -\langle T_\tau S_0^+(\tau) S_j^-(0) \rangle, \tag{2}$$

where $S_{j}^{\pm}=S_{j}^{x}\pm iS_{j}^{y}$ and $A\left(au\right)$ is defined as $A\left(au\right) =e^{ au H}Ae^{- au H}$ for any operator A. 0 represents a site in the bulk of the system.

In order to systematically compute the equation of motion, we first present a general formula. Suppose A and B represent the products of spin operators. We define the following Green's function:

$$G_{AB}(\tau) = -\langle T_{\tau}A(\tau)B(0)\rangle \equiv \langle A|B\rangle_{\tau}.$$
 (3)

The equation of motion is given by

$$\frac{\partial}{\partial \tau} \mathcal{G}_{AB}(\tau) = -\langle T_{\tau} [H, A(\tau)] B(0) \rangle - \delta(\tau) \langle [A, B] \rangle. \quad (4)$$

The Fourier transform of $\mathcal{G}_{AB}\left(\tau\right)$ is defined by:

$$\mathcal{G}_{AB}(i\omega_n) = \int_0^\beta d\tau e^{i\omega_n \tau} \langle A|B\rangle_\tau \equiv \langle A|B\rangle_{i\omega_n}. \quad (5)$$
Here the bosonic Matsubara frequency ω_n takes the val-

Here the bosonic Matsubara frequency ω_n takes the values $\omega_n = \frac{2\pi n}{\beta}$, where n is an integer, and $\beta = \frac{1}{k_{\rm B}T}$ is the inverse temperature with $k_{\rm B}$ being the Boltzmann constant and T being the temperature. After the Fourier transformation of Eq. (4), we obtain the following equation:

$$i\omega_{n}\langle A|B\rangle_{i\omega_{n}}=\langle [A,H]|B\rangle_{i\omega_{n}}+\langle [A,B]\rangle\,. \eqno(6)$$

This is the general equation of motion. We can use Eq. (6) with A replaced by [A,H] to derive the equation of motion for the first term in the right-hand side. By repeating similar steps, we can derive higher-order equations of motion. Furthermore, by rewriting Eq. (3) as:

$$\mathcal{G}_{AB}(\tau) = -\langle T_{\tau} A(0) B(-\tau) \rangle, \qquad (7)$$

we can derive the following equation of motion[9]:

$$i\omega_{n}\langle A|B\rangle_{i\omega_{n}}=-\langle A\mid [B,H]\rangle_{i\omega_{n}}+\langle [A,B]\rangle\,. \eqno(8)$$

Applying Eq. (6) to Eq. (2) and computing $[S_0^+, H]$ we obtain the following equation of motion:

$$i\omega_n \langle S_0^+ | S_j^- \rangle_{i\omega_n} = J_{\delta_1} \langle S_0^z S_1^+ | S_j^- \rangle_{i\omega_n} - J_{\delta_1} \langle S_0^+ S_1^z | S_j^- \rangle_{i\omega_n}.$$
(9)

Here, we assume that the SU(2) symmetry in spin space is not broken so that

$$\langle \left[S_0^+, S_j^- \right] \rangle = 2\delta_{j,0} \langle S_0^z \rangle = 0.$$
 (10)

In Eq. (9), we denote 1 as the site interacting with site 0, and δ_1 represents the displacement vector connecting site 0 and site 1. The summation with respect to site 1 is implicit to simplify the notation.

The equation of motions for the two terms in the right hand side of Eq. (9) are

$$i\omega_{n} \langle S_{0}^{z} S_{1}^{+} | S_{j}^{-} \rangle_{i\omega_{n}} = J_{\delta_{2}} \langle S_{0}^{z} S_{1}^{z} S_{1+2}^{+} | S_{j}^{-} \rangle_{i\omega_{n}} - J_{\delta_{2}} \langle S_{0}^{z} S_{1}^{+} S_{1+2}^{z} | S_{j}^{-} \rangle_{i\omega_{n}} + \frac{1}{2} J_{\delta_{2}} \langle S_{0}^{+} S_{2}^{-} S_{1}^{+} | S_{j}^{-} \rangle_{i\omega_{n}} - \frac{1}{2} J_{\delta_{2}} \langle S_{0}^{-} S_{2}^{+} S_{1}^{+} | S_{j}^{-} \rangle_{i\omega_{n}} + 2 \delta_{1,j} \langle S_{0}^{z} S_{1}^{z} \rangle - \delta_{0,j} \langle S_{0}^{-} S_{1}^{+} \rangle,$$

$$(11)$$

and

$$i\omega_{n}\langle S_{0}^{+}S_{1}^{z}|S_{j}^{-}\rangle_{i\omega_{n}} = \frac{1}{2}J_{\delta_{2}}\langle S_{0}^{+}S_{1}^{+}S_{1+2}^{-}|S_{j}^{-}\rangle_{i\omega_{n}} - \frac{1}{2}J_{\delta_{2}}\langle S_{0}^{+}S_{1}^{-}S_{1+2}^{+}|S_{j}^{-}\rangle_{i\omega_{n}} + J_{\delta_{2}}\langle S_{0}^{z}S_{2}^{+}S_{1}^{z}|S_{j}^{-}\rangle_{i\omega_{n}} - J_{\delta_{2}}\langle S_{0}^{+}S_{1}^{z}S_{j}^{z}\rangle_{i\omega_{n}} - \delta_{1,j}\langle S_{0}^{+}S_{1}^{-}\rangle + 2\delta_{0,j}\langle S_{0}^{z}S_{1}^{z}\rangle.$$

$$(12)$$

Here, 1+2 represents the site $\delta_1 + \delta_2$. It is important to note that sites 1 and 2 can be the same site in this expression.

Now we apply the decoupling approximation introduced by Kondo and Yamaji[8]. That is, for example,

$$\langle S_0^z S_1^z S_2^+ | S_j^- \rangle_{i\omega_n} \simeq \alpha \langle S_0^z S_1^z \rangle \langle S_2^+ | S_j^- \rangle_{i\omega_n}, \tag{13}$$

After applying this decoupling scheme, we obtain

where α is a parameter to be determined. This is understood as follows[8]:

$$\langle S_0^z S_1^z S_2^+ | S_j^- \rangle_{i\omega_n} = \langle S_0^z S_1^z \left[\alpha + 2 \left(1 - \alpha \right) S_2^z \right] S_2^+ | S_j^- \rangle_{i\omega_n}$$

$$\simeq \langle S_0^z S_1^z \left[\alpha + 2 \left(1 - \alpha \right) S_2^z \right] \rangle \langle S_2^+ | S_j^- \rangle_{i\omega_n}$$

$$= \alpha \langle S_0^z S_1^z \rangle \langle S_2^+ | S_j^- \rangle_{i\omega}. \tag{14}$$

$$i\omega_{n}\mathcal{F}_{j}(i\omega_{n})$$

$$\simeq \frac{1}{2}\left[(1-\delta_{1,2})J_{\delta_{2}}\alpha c_{1-2} + \delta_{1,2}J_{\delta_{1}}\right]\mathcal{G}_{j}(i\omega_{n}) - \frac{1}{2}\left[(1-\delta_{1+2,0})J_{\delta_{2}}\alpha c_{1+2} + \delta_{1+2,0}J_{\delta_{2}}\right]\mathcal{G}_{j-1}(i\omega_{n})$$

$$+ \frac{1}{2}\left(1-\delta_{1+2,0}\right)J_{\delta_{2}}\alpha c_{1}\mathcal{G}_{j-1-2}(i\omega_{n}) - \frac{1}{2}\left(1-\delta_{1,2}\right)J_{\delta_{2}}\alpha c_{1}\mathcal{G}_{j-2}(i\omega_{n})$$

$$- \frac{1}{2}\delta_{1+2,0}J_{\delta_{2}}\mathcal{F}_{j}(i\omega_{n}) + \frac{1}{2}\delta_{1,2}J_{\delta_{1}}\mathcal{F}_{j}(i\omega_{n}) + (\delta_{1,j}-\delta_{0,j})c_{1},$$
(15)

where

$$\mathcal{F}_{j}\left(i\omega_{n}\right) = \left\langle S_{0}^{z}S_{1}^{+} \mid S_{j}^{-}\right\rangle_{i\omega_{n}} - \left\langle S_{0}^{+}S_{1}^{z} \mid S_{j}^{-}\right\rangle_{i\omega_{n}}. \quad (16)$$

Here, we defined the spin correlation function by the following equation:

$$c_{i-j} = c_{j-i} \equiv 2\langle S_i^+ S_j^- \rangle = 4\langle S_i^z S_j^z \rangle. \tag{17}$$

After the Fourier transformation,

$$\mathcal{G}_{k}(i\omega_{n}) = \sum_{j} e^{-i\mathbf{k}\cdot\mathbf{R}_{j}} \mathcal{G}_{j}(i\omega_{n}), \qquad (18)$$

$$\mathcal{F}_{k}(i\omega_{n}) = \sum_{j} e^{-i\mathbf{k}\cdot\mathbf{R}_{j}} \mathcal{F}_{j}(i\omega_{n}), \qquad (19)$$

where \mathbf{R}_{i} represents the coordinate of site j, we obtain

$$i\omega_{n} \begin{pmatrix} \mathcal{G}_{\mathbf{k}} (i\omega_{n}) \\ \mathcal{F}_{\mathbf{k}} (i\omega_{n}) \end{pmatrix} \simeq \begin{pmatrix} 0 & J_{\boldsymbol{\delta}_{1}} \\ K_{\mathbf{k}} & 0 \end{pmatrix} \begin{pmatrix} \mathcal{G}_{\mathbf{k}} (i\omega_{n}) \\ \mathcal{F}_{\mathbf{k}} (i\omega_{n}) \end{pmatrix} + \begin{pmatrix} 0 \\ (e^{i\mathbf{k}\cdot\boldsymbol{\delta}_{1}} - 1) c_{1} \end{pmatrix}, \quad (20)$$

where

$$K_{\mathbf{k}} = \frac{1}{2} \left[(1 - \delta_{1,2}) J_{\delta_{2}} \alpha c_{1-2} + \delta_{1,2} J_{\delta_{1}} \right]$$

$$- \frac{1}{2} \left[(1 - \delta_{1+2,0}) J_{\delta_{2}} \alpha c_{1+2} + \delta_{1+2,0} J_{\delta_{2}} \right] e^{i\mathbf{k} \cdot \delta_{1}}$$

$$- \frac{1}{2} (1 - \delta_{1,2}) J_{\delta_{2}} \alpha c_{1} e^{i\mathbf{k} \cdot \delta_{2}}$$

$$+ \frac{1}{2} (1 - \delta_{1+2,0}) J_{\delta_{2}} \alpha c_{1} e^{i\mathbf{k} \cdot (\delta_{1} + \delta_{2})}.$$

$$(21)$$

By solving Eq. (20) with respect to $\mathcal{G}_{\mathbf{k}}(i\omega_n)$, we obtain

$$\mathcal{G}_{\mathbf{k}}(i\omega_n) = \frac{J_{\boldsymbol{\delta}_1} \left(e^{i\mathbf{k}\cdot\boldsymbol{\delta}_1} - 1 \right) c_1}{\left(i\omega_n \right)^2 - \omega_{\mathbf{k}}^2}, \tag{22}$$

where

$$\omega_{\mathbf{k}}^{2} = \frac{1}{2} J_{\delta_{1}} \left[(1 - \delta_{1,2}) J_{\delta_{2}} \alpha c_{1-2} \right]
- \frac{1}{2} J_{\delta_{1}} \left[(1 - \delta_{1+2,0}) J_{\delta_{2}} \alpha c_{1+2} + \delta_{1+2,0} J_{\delta_{2}} \right] e^{i\mathbf{k} \cdot \delta_{1}}
- \frac{1}{2} (1 - \delta_{1,2}) J_{\delta_{1}} J_{\delta_{2}} \alpha c_{1} e^{i\mathbf{k} \cdot \delta_{2}}
+ \frac{1}{2} (1 - \delta_{1+2,0}) J_{\delta_{1}} J_{\delta_{2}} \alpha c_{1} e^{i\mathbf{k} \cdot (\delta_{1} + \delta_{2})}.$$
(23)

Equations (22) and (23) provide us with the general formula. When applying this formula to a specific system, we only need to perform the necessary summations with

respect to 1 and 2, which are implicit in the equations above. This allows us to efficiently compute the Green's function and the corresponding frequency for the given spin system without the need to derive the equations from scratch each time.

The correlation functions c_{i-j} are determined through a self-consistent calculation. The Fourier transform of $\mathcal{G}_{\mathbf{k}}(i\omega_n)$ leads to

$$\mathcal{G}_{\mathbf{k}}(\tau) = \frac{1}{\beta} \sum_{i\omega_n} e^{-i\omega_n \tau} \mathcal{G}_{\mathbf{k}}(i\omega_n)
= \frac{A_{\mathbf{k}}}{2\omega_{\mathbf{k}}} \left(\frac{e^{-\tau\omega_{\mathbf{k}}}}{e^{-\beta\omega_{\mathbf{k}}} - 1} - \frac{e^{\tau\omega_{\mathbf{k}}}}{e^{\beta\omega_{\mathbf{k}}} - 1} \right), \quad (24)$$

where

$$A_{\mathbf{k}} = J_{\boldsymbol{\delta}_1} \left(e^{i\mathbf{k} \cdot \boldsymbol{\delta}_1} - 1 \right) c_1 \tag{25}$$

The correlation function is given by

$$c_j = 2 \left\langle S_0^+ S_j^- \right\rangle = \frac{1}{N} \sum_{\mathbf{k}} e^{i\mathbf{k}\cdot\mathbf{R}_j} \frac{A_{\mathbf{k}}}{\omega_{\mathbf{k}}} \coth\left(\frac{\beta\omega_{\mathbf{k}}}{2}\right).$$
 (26)

If we introduce a single decoupling parameter α at Eq. (13), the total number of parameters to be determined, including α , is equal to the number of selfconsistent equations that need to be solved. This can be achieved by utilizing the identity $c_0 = 1$. However, if additional decoupling parameters are introduced, we must impose extra conditions or constraints on the system to guarantee a unique solution. These additional conditions can be other theoretical results and/or experimental findings. We do not introduce additional decoupling parameters, and employ a single decoupling parameter. Consequently, the system of equations can be solved independently without requiring any extra conditions. This self-contained nature of the formalism streamlines the solution process, making it more efficient and eliminating the need for additional constraints or conditions, which is particularly advantageous in practical applications.

Now we present formula for thermodynamical quantities. The energy of the system is given by

$$E = \sum_{\langle i,j \rangle} J_{ij} \langle \mathbf{S}_i \cdot \mathbf{S}_j \rangle = \frac{3}{4} N \sum_j J_{0j} c_j.$$
 (27)

By taking the derivative of E with respect to the temperature, T, we obtain the specific heat. The uniform spin susceptibility is given by

$$\chi = \frac{\beta(g\mu_B)^2}{N} \sum_{i,j} \langle S_i^z S_j^z \rangle = \frac{\beta(g\mu_B)^2}{2N} \sum_{i,j} \langle S_i^+ S_j^- \rangle$$
$$= \frac{\beta(g\mu_B)^2}{4} \sum_j c_j. \tag{28}$$

Here, g is the g-factor and μ_B is the Bohr magneton. Note that there is relationship between $\langle S_i^+ S_j^- \rangle$ and $\langle S_j^z S_j^z \rangle$ because of the SU(2) symmetry in spin space. The formula for χ corresponds to the spin susceptibility obtained by taking the average of the longitudinal spin susceptibility and the transverse spin susceptibility, that corresponds to the spin susceptibility of powder samples experimentally. Substituting Eq. (26) into Eq. (28), we obtain

$$\chi = \frac{\beta (g\mu_B)^2}{4} \lim_{\mathbf{k} \to 0} \frac{A_{\mathbf{k}}}{\omega_{\mathbf{k}}} \coth\left(\frac{\beta \omega_{\mathbf{k}}}{2}\right). \tag{29}$$

When the spatial dimension d is $d \geq 3$, the theory describes the magnetic long-range order at finite temperature. Suppose that $\omega_{\mathbf{k}} = 0$ at $\mathbf{k} = \mathbf{Q}$ when $T \leq T_c$. In this case Bose-Einstein condensation occurs at $\mathbf{k} = \mathbf{Q}$, and Eq. (26) is rewritten as

$$c_{j} = 2 \left\langle S_{0}^{+} S_{j}^{-} \right\rangle$$

$$= \frac{1}{N} \sum_{\mathbf{k}(\neq \mathbf{Q})} e^{i\mathbf{k} \cdot \mathbf{R}_{j}} \frac{A_{\mathbf{k}}}{\omega_{\mathbf{k}}} \coth\left(\frac{\beta \omega_{\mathbf{k}}}{2}\right) + e^{i\mathbf{Q} \cdot \mathbf{R}_{j}} n_{\mathbf{Q}}(30)$$

where $n_{\mathbf{Q}}$ is associated with the component of Bose-Einstein condensation at $\mathbf{k} = \mathbf{Q}$. Multiplying $e^{-i\mathbf{Q}\cdot\mathbf{R}_j}$ and taking $\mathbf{R}_j \to \infty$ limit, we obtain

$$\lim_{\mathbf{R}_{j}\to\infty} e^{-i\mathbf{Q}\cdot\mathbf{R}_{j}} c_{j} = 2 \lim_{\mathbf{R}_{j}\to\infty} e^{-i\mathbf{Q}\cdot\mathbf{R}_{j}} \left\langle S_{0}^{+} S_{j}^{-} \right\rangle = n_{\mathbf{Q}}.$$
(31)

This equation implies the presence of the magnetic long-range order with the wavelength Q:

$$\langle \mathbf{S}_j \rangle = e^{i\mathbf{Q} \cdot \mathbf{R}_j} \mathbf{m}_{\mathbf{Q}},$$
 (32)

where

$$|\boldsymbol{m}_{\boldsymbol{Q}}| = \sqrt{\frac{3}{4}n_{\boldsymbol{Q}}}.\tag{33}$$

Note that there is no specific direction for m_Q in our formulation because of SU(2) symmetry in spin space. For $T < T_c$ we need to solve the self-consistent equation with including n_Q . Here, we assumed that the wave vector for the magnetic long-range order is specified by the single wave vector Q, for simplicity. It is easy to extend the formula to the magnetic long-ranger oder with multiple wave vectors.

III. d-DIMENSIONAL HYPERCUBIC LATTICE

In this section, we shall derive the formula for the hypercubic lattice with a spatial dimension d. We show that for d = 1 and d = 2, our formula yields accurate results at high temperatures, and for d = 3, it predicts the transition temperature with greater precision than mean field theory, closely aligning with the quantum Monte Carlo results. We make the assumption that $J_{ij} = J$ if sites i and j are nearest neighbors, and $J_{ij} = 0$ otherwise.

By performing the implicit summations in Eq. (23), we obtain

$$\omega_{\mathbf{k}}^{2} = \frac{1}{2} J^{2} z (1 - \gamma_{\mathbf{k}}) \left[1 - (1 + z \gamma_{\mathbf{k}}) a_{1} + (z - 2) a_{11} + a_{2} \right],$$
(34)

where z = 2d, $a_1 = \alpha c_1$ etc., and

$$\gamma_{\mathbf{k}} = \frac{1}{d} \sum_{\mu=1}^{d} \cos k_{\mu}. \tag{35}$$

Here, we set the lattice constant to unity. The Green's function is given by

$$\mathcal{G}_{\mathbf{k}}(i\omega_n) = -\frac{Jz\left(1 - \gamma_{\mathbf{k}}\right)c_1}{\left(i\omega_n\right)^2 - \omega_{\mathbf{k}}^2}.$$
 (36)

We note that this result includes the one-dimensional chain [8] and the two-dimensional square lattice [10].

The self-consistent equations are given by

$$1 = -\frac{zc_1J}{N} \sum_{\mathbf{k}} \frac{1 - \gamma_{\mathbf{k}}}{\omega_{\mathbf{k}}} \coth\left(\frac{\beta\omega_{\mathbf{k}}}{2}\right), \quad (37)$$

$$c_1 = -\frac{zc_1J}{N} \sum_{\mathbf{k}} \gamma_{\mathbf{k}} \frac{1 - \gamma_{\mathbf{k}}}{\omega_{\mathbf{k}}} \coth\left(\frac{\beta\omega_{\mathbf{k}}}{2}\right), \quad (38)$$

$$(z-2) c_{11} + c_2 = -\frac{zc_1 J}{N} \sum_{\mathbf{k}} \left(z \gamma_{\mathbf{k}}^2 - 1 \right) \times \frac{1 - \gamma_{\mathbf{k}}}{\omega_{\mathbf{k}}} \coth\left(\frac{\beta \omega_{\mathbf{k}}}{2} \right). \quad (39)$$

Here, c_{11} represents the correlation function between sites with a real space displacement vector of $(\pm 1, \pm 1)$ for d = 2 and $(\pm 1, \pm 1, 0)$, $(\pm 1, 0, \pm 1)$, and $(0, \pm 1, \pm 1)$ for d = 3. For d = 1, the left hand side of Eq. (39) is reduced to c_2 and concurrently, the coefficient of a_{11} vanishes in the right hand side of Eq. (34) due to z = 2. Therefore, c_{11} is irrelevant for d = 1.

Figure 1 shows the temperature dependence of the energy and specific heat for the case of d=1. This result is benchmarked against the exact diagonalization result for a system of 10 spins. The Green's function approach aligns exceptionally well with the exact diagonalization result at high temperatures. However, it deviates from the exact result as the temperature lowers. The specific heat peak is overestimated by approximately 16 percent compated with the transfer-matrix renormalization-group method[11]. Detailed discussions comparing the theory with high-temperature expansions and the results for the ferromagnetic case are provided in ref. 8.

Figure 2 displays the temperature dependence of the spin susceptibility for the case of d=2. The Green's function theory is benchmarked against the quantum Monte Carlo results[12, 13]. At high temperatures, the Green's function theory closely matches the quantum

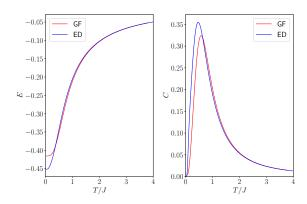


FIG. 1. (Color online) Comparison of the Green's function theory (GF) for the case of d=1 with the exact diagonalization result (ED) for a system of 10 spins: the left panel displays the energy of the system, while the right panel presents the specific heat.

Monte Carlo results, particularly for the peak position of the susceptibility. However, notable discrepancies arise at low temperatures. Methods to improve these results are discussed in ref. 10, which includes a discussion on Bose-Einstein condensation at zero temperature. Leveraging the accurate peak position estimation provided by the Green's function approach, the magnetic torque experiments in cuprate high-temperature superconductors are satisfactorily analyzed in ref. 14.

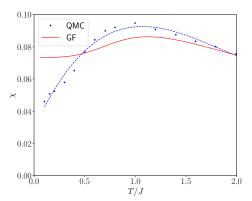


FIG. 2. (Color online) Temperature dependence of the spin susceptibility, measured in units of $(g\mu_{\rm B})^2/J$, predicted by the Green's function theory (GF) for the case of d=2, compared with the quantum Monte Carlo results (QMC)[12]. For the latter, the linear size of the system is L=12, which is consistent with results obtained for larger L[13]. The dashed line is a guide for the eyes.

We now consider the case of d=3. In this case, the Green's function theory accounts for the antiferromagnetic phase transition at finite temperature. Antiferromagnetic long-range order occurs when $\omega_{\mathbf{Q}}$ vanishes, where $\mathbf{Q}=(\pi,\pi,\pi)$.

Figure 3 presents the temperature dependencies of the

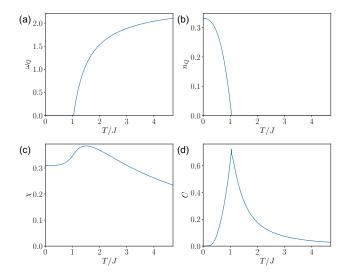


FIG. 3. (Color online) Temperature dependencies for the case of d=3 showing (a) the gap $\omega_{\mathbf{Q}}$, (b) the Bose-Einstein condensate component $n_{\mathbf{Q}}$, (c) the spin susceptibility, and (d) the specific heat. Here, $\omega_{\mathbf{Q}}$ is measured in units of J, χ in units of $(g\mu_{\mathrm{B}})^2/(6J)$, and C in units of $Nk_{\mathrm{B}}J$.

gap $\omega_{\boldsymbol{Q}}$, the Bose-Einstein condensate component $n_{\boldsymbol{Q}}$, the spin susceptibility, and the specific heat. To estimate the transition temperature, we performed calculations for various values of the number of points in the Brillouin zone, $N_{\rm BZ} \equiv N_k^3$. Fitting the results to the function $T_c(N_k) = a + b/N_k + c/N_k^2$ with a, b, and c as fitting parameters, we obtained $T_c = 1.039$, which agrees with the previous result[15]. This value closely matches the quantum Monte Carlo result[16] of $T_c/J = 0.946$. Since

SU(2) symmetry in spin space is preserved in the theory, the spin susceptibility is the average of the longitudinal and transverse spin susceptibilities as stated above. The specific heat exhibits a peak at the transition temperature

IV. THE J_1 - J_2 MODEL

In the investigation of quantum spin liquid states, the influence of frustration effects is significant. To assess the viability of the Green's function approach for addressing frustrated spin systems, we turn our attention to the J_1 - J_2 model on the square lattice[17–26]. In this model, J_1 denotes the interaction between nearest neighbors, while J_2 denotes the interaction between next-nearest neighbors. This system demonstrates characteristics of frustration, and it has been hypothesized that a quantum spin liquid phase emerges around the ratio $J_2/J_1 = 1/2$ [17]. Recent studies employing machine learning methodologies [26] have suggested that this spin liquid state is realized within the range of $0.49 \le$ $J_2/J_1 \leq 0.54$. Meanwhile, investigations utilizing tensor network approaches has indicated [27] potential C_{4v} symmetry breaking at $T/J_1 \sim 0.1$ when $J_2 \sim J_1$.

In the following, we investigate this model at both zero and finite temperatures. Although a discussion of the conditions for the spin liquid state is precluded due to the limitations of the second-order approximation used in this study, we can nonetheless gain insights into C_{4v} symmetry breaking or nematic correlations by considering the anisotropy of spin correlations.

By employing the derived formula above, we obtain the following results:

$$\omega_{\mathbf{k}}^{2} = 2J_{1}^{2} \left[(1 + a_{2} + 2a_{11}) - (1 + 4\gamma_{\mathbf{k}}) a_{1s} \right] (1 - \gamma_{\mathbf{k}}) + 2J_{1}^{2} \gamma_{\mathbf{k}}^{a} (1 + 4\gamma_{\mathbf{k}}) a_{1a}$$

$$+ 2J_{2}^{2} (1 - \gamma_{\mathbf{k}}') \left[(1 + a_{22} + 2a_{2}) - a_{11} (1 + 4\gamma_{\mathbf{k}}') \right]$$

$$+ 4J_{1}J_{2} \left[(1 - \gamma_{\mathbf{k}}) + (1 - \gamma_{\mathbf{k}}') - 2\gamma_{\mathbf{k}}' (1 - \gamma_{\mathbf{k}}) \right] a_{1s} + 4J_{1}J_{2} \gamma_{\mathbf{k}}^{a} (1 + 2\gamma_{\mathbf{k}}') a_{1a}$$

$$+ 4J_{1}J_{2} \left[(1 - \gamma_{\mathbf{k}}) + (1 - \gamma_{\mathbf{k}}') \right] a_{21s} - 4J_{1}J_{2} \gamma_{\mathbf{k}}^{a} a_{21a} - 8J_{1}J_{2} \gamma_{\mathbf{k}} (1 - \gamma_{\mathbf{k}}') a_{11},$$

$$(40)$$

where $\gamma_{\mathbf{k}} = (\cos k_x + \cos k_u)/2$,

$$\gamma_{\mathbf{k}}' = \cos k_x \cos k_y,\tag{41}$$

$$\gamma_{\mathbf{k}}^{a} = \frac{1}{2} \left(\cos k_x - \cos k_y \right), \tag{42}$$

and $a_{1s} = (a_{1x} + a_{1y})/2$, $a_{1a} = (a_{1x} - a_{1y})/2$, $a_{21s} = (a_{21x} + a_{21y})/2$, $a_{21a} = (a_{21x} - a_{21y})/2$. $a_{1x} (a_{1y})$ refers to the nearest neighbor correlation function in the x(y) direction. Similarly, $a_{21x} (a_{21y})$ denotes the correlation function between the sites separated by the displacement vector (2,1) ((1,2)). The variables a_{1a} and a_{21a} are associated with C_{4v} symmetry breaking. When a_{1a} and

 a_{21a} are non-vanishing, that indicates the presence of nematic correlations in the system. We note that Eq. (40), when excluding these nematic correlations, agrees with the previous result[28]. The self-consistent equations are

given by

$$\alpha = a_{1s}I_{00}^{(0)} + a_{1a}I_{00}^{(1)} + a_{11}I_{00}^{(2)}, \tag{43}$$

$$a_{1s} = a_{1s}I_{1s}^{(0)} + a_{1a}I_{1s}^{(1)} + a_{11}I_{1s}^{(2)},$$
 (44)

$$a_{1a} = a_{1s}I_{1a}^{(0)} + a_{1a}I_{1a}^{(1)} + a_{11}I_{1a}^{(2)},$$
 (45)

$$a_{11} = a_{1s}I_{11}^{(0)} + a_{1a}I_{11}^{(1)} + a_{11}I_{11}^{(2)},$$
 (46)

$$a_2 = a_{1s}I_{20}^{(0)} + a_{1a}I_{20}^{(1)} + a_{11}I_{20}^{(2)},$$
 (47)

$$a_{21s} = a_{1s}I_{21s}^{(0)} + a_{1a}I_{21s}^{(1)} + a_{11}I_{21s}^{(2)},$$
 (48)

$$a_{21a} = a_{1s}I_{21a}^{(0)} + a_{1a}I_{21a}^{(1)} + a_{11}I_{21a}^{(2)},$$
 (49)

$$a_{22} = a_{1s}I_{22}^{(0)} + a_{1a}I_{22}^{(1)} + a_{11}I_{22}^{(2)},$$
 (50)

where

$$I_{\eta}^{(\ell)} = -\frac{8J^{(\ell)}}{\beta N} \sum_{\mathbf{k}} f_{\eta}(\mathbf{k}) \, \sigma_{\mathbf{k}}^{(\ell)} g\left(\frac{\beta \omega_{\mathbf{k}}}{2}\right), \tag{51}$$

with $J^{(0)} = J^{(1)} = J_1$, $J^{(2)} = J_2$, $g(x) = x \coth x$, and

$$\sigma_{\mathbf{k}}^{(0)} = \frac{1 - \gamma_{\mathbf{k}}}{\omega_{\mathbf{k}}^2}, \tag{52}$$

$$\sigma_{\mathbf{k}}^{(1)} = -\frac{\gamma_{\mathbf{k}}^a}{\omega_{\mathbf{k}}^2},\tag{53}$$

$$\sigma_{\mathbf{k}}^{(2)} = \frac{1 - \gamma_{\mathbf{k}}'}{\omega_{\mathbf{k}}^2}.\tag{54}$$

The function $f_{\eta}(\mathbf{k})$ are defined by

$$f_{00}\left(\boldsymbol{k}\right) = 1,\tag{55}$$

$$f_{1s}(\mathbf{k}) = \gamma_{\mathbf{k}}, \tag{56}$$

$$f_{1a}\left(\boldsymbol{k}\right) = \gamma_{\boldsymbol{k}}^{a},\tag{57}$$

$$f_{11}(\mathbf{k}) = \gamma_{\mathbf{k}}, \tag{51}$$

$$f_{11}(\mathbf{k}) = \gamma_{\mathbf{k}}', \tag{58}$$

(58)

$$f_{20}(\mathbf{k}) = 4\gamma_{\mathbf{k}}^2 - 2\gamma_{\mathbf{k}}' - 1,$$
 (59)

$$f_{21s}\left(\mathbf{k}\right) = \gamma_{\mathbf{k}} \left(2\gamma_{\mathbf{k}}' - 1\right), \tag{60}$$

$$f_{21a}\left(\mathbf{k}\right) = \gamma_{\mathbf{k}}^{a}\left(2\gamma_{\mathbf{k}}'+1\right),\tag{61}$$

$$f_{22}(\mathbf{k}) = 4{\gamma_{\mathbf{k}}'}^2 - 8{\gamma_{\mathbf{k}}}^2 + 4{\gamma_{\mathbf{k}}'} + 1.$$
 (62)

We solve the self-consistent equations (43) to (50) as follows: Initially, we solve the equations for r=0, resulting in a reduced set of equations that simplifies to a single equation. This equation can be solved using the bisection method. Subsequently, we solve the differential equations for a_{ij} , employing either the parameter r or the temperature T as the variable. Notably, it is unnecessary to compute α at intermediary steps. The change in α concerning r or T can be calculated at the end of the computation.

Figure 4 presents the results at temperature T=0. The correlation functions are plotted as a function of the ratio $r = J_2/J_1$. It is worth noting that there exists a symmetry between the cases r = 0 and r = 1, as previously observed [28], due to the exchange between J_1 and J_2 . Additionally, we observe that the nematic correlations $c_{1a} = a_{1a}/\alpha$ and $c_{21a} = a_{21a}/\alpha$ are both zero within

the numerical error. The formula derived in this study was obtained by employing the decoupling scheme at the second-order equation of motion. Within this approximation, the right hand side of Eq. (51) diverges at T=0when the spin-wave gap associated with the long-range order vanishes. Therefore, the self-consistent equations at T=0 do not directly allow us to discuss the presence of long-range order. However, within this framework, we can investigate the short-range order. Based on our analysis of the self-consistent equations, we find no indication of short-range nematic correlation in the system.

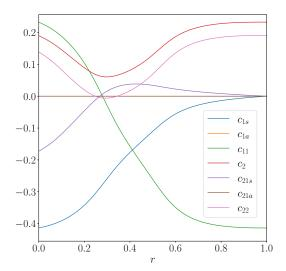


FIG. 4. (Color online) Spin correlation functions as a function of $r = J_2/J_1$ at T = 0. There is symmetry between the correlation functions at r=0 and those at r=1. Specifically, c_1 , c_{11} , and c_2 at r=0 correspond to c_{11} , c_2 , and c_{22} at r=1, respectively. The results confirm this symmetry. Additionally, the nematic correlations, c_{1a} and c_{21a} , are found to be zero within the numerical error.

The spin-wave dispersion at T=0 is shown in Fig. 5. There is a systematic change in the energy dispersion by varying the values of J_1 and J_2 . It is important to note that there is no need to assume any long-range order to obtain the spin-wave dispersion. However, a discrepancy arises when considering the gap at (π, π) and $(\pi, 0)$. For the case when J_1 is finite and $J_2 = 0$, the gap at (π, π) should vanish, and similarly, for $J_1 = 0$ and J_2 is finite, the gap at $(\pi,0)$ should also vanish. However, the decoupling approximation at the second-order equation of motion, as mentioned earlier, leads to a finite gap at these points, contradicting the expected behavior. Employing the decoupling scheme at the third-order equation of motion has the potential to yield improvements and could resolve the discrepancy observed in the gap at (π, π) and $(\pi,0)$. Such investigations are left for future research. One can also compute the energy dispersion at finite temperature without long-range order but with short-range order. The advantage of this formula is that it enables

the computation of dynamical quantities, which can be experimentally verified.

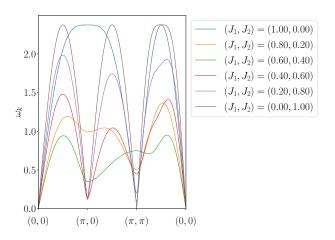


FIG. 5. (Color online) Spin-wave dispersion along the high-symmetric lines in the Brillouin zone for different values of J_1 and J_2 . Here, the values of J_1 , J_2 , and ω_k are expressed in units of J, which is taken as the unit of energy.

We now investigate the model at finite temperatures. We expect the Green's function approach to become accurate at high temperatures due to the short spin-spin correlation length. This is explicitly demonstrated for the one-dimensional system and the square lattice case above. Therefore, in principle, we can utilize the high-temperature expansion result[29] to set the initial values of the correlation functions, c_{ij} , when solving the self-consistent equations. The high-temperature expansion results for the correlation functions, up to the second order in β , are given by:

$$c_{1s} = -\frac{1}{4}\beta J_1 - \frac{1}{16}\beta^2 J_1^2 + \frac{1}{8}\beta^2 J_1 J_2, \qquad (63)$$

$$c_{11} = -\frac{1}{4}\beta J_2 + \frac{1}{8}\beta^2 J_1^2, \tag{64}$$

$$c_2 = \frac{1}{16}\beta^2 J_1^2 + \frac{1}{8}\beta^2 J_2^2, \tag{65}$$

$$c_{21s} = \frac{1}{8}\beta^2 J_1 J_2, \tag{66}$$

$$c_{22} = \frac{1}{16} \beta^2 J_2^2. (67)$$

Figure 6 presents the correlation functions compared with the results from high-temperature expansions. The concordance is excellent at elevated temperatures.

In principle, one can perform a self-consistent calculation by initializing the correlation functions with the high-temperature expansion results and then progressively lowering the temperature. This method is particularly effective when the effects of frustration are weak. For the cases of $(J_1, J_2) = (1, 0), (0.9, 0.1), (0.8, 0.2)$ and $(J_1, J_2) = (0, 1), (0.1, 0.9), (0.2, 0.8)$, we achieved satisfactory results. The former is shown in Fig. 7 and the latter

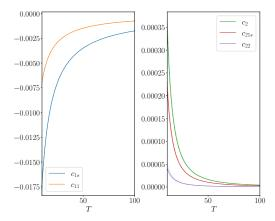


FIG. 6. (Color online) Temperature dependence of the correlation functions (dotted lines) compared with the high-temperature expansion results, given by Eqs. (63) to (67) (solid lines), for $J_1 = 0.7$ and $J_2 = 0.3$. The temperature range is $10 \le T \le 100$.

in Fig. 8, where the temperature dependencies of the specific heat, spin susceptibility, and gaps at characteristic wave vectors are shown. Here, χ and C are measured in units of $(g\mu_{\rm B})^2/J$ and $Nk_{\rm B}J$, respectively, where J represents the unit of energy. The gaps are defined as $\Delta(\pi,\pi) = \omega_{(\pi,\pi)}$ and $\Delta(\pi,0) = \omega_{(\pi,0)}$. In the case of small J_2 , as shown in Fig. 7, the peak in the specific heat shifts to lower temperatures with an increase in J_2 , while simultaneously reducing the peak value. This shift is also observed in the spin susceptibility. This trend can be interpreted as the suppression of the antiferromagnetic correlation with the wave vector (π, π) due to the increase in J_2 . This interpretation aligns with the behavior of $\Delta(\pi,\pi)$, which increases as J_2 increases, indicating that the antiferromagnetic correlation becomes more short-ranged. Meanwhile, $\Delta(\pi,0)$ decreases with an increase in J_2 , suggesting a slight enhancement of the antiferromagnetic correlation with the wave vector $(\pi, 0)$.

In the case of small J_1 , as depicted in Fig. 8, the peak in the specific heat shifts to lower temperatures with an increase in J_1 . Unlike the case with small J_2 , the peak value remains almost unchanged. This shift is also observed in the spin susceptibility, interpreted as the suppression of the antiferromagnetic correlation with the wave vector $(\pi,0)$ due to the increase in J_1 . For the case of $(J_1,J_2)=(0,1)$, the gap $\Delta(\pi,\pi)$ is identically zero. $\Delta(\pi,\pi)$ becomes finite and increases as J_1 increases. Meanwhile, $\Delta(\pi,0)$ shows almost no change. This behavior suggests that the system is close to the antiferromagnetic long-range ordered state with the wave vector $(\pi,0)$.

Now we consider the cases with strong frustration. When the effects of frustration are pronounced, extremely precise numerical computations become necessary[29]. In fact the procedure of starting from high temperatures and low-

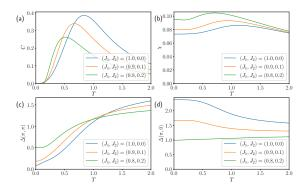


FIG. 7. (Color online) Temperature dependencies for (a) the specific heat, (b) the spin susceptibility, (c) the gap at (π, π) , and (d) the gap at $(\pi, 0)$ for the cases of $(J_1, J_2) = (1.0, 0.0), (0.9, 0.1), (0.8, 0.2)$.

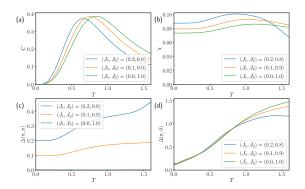


FIG. 8. (Color online) Temperature dependencies for (a) the specific heat, (b) the spin susceptibility, (c) the gap at (π, π) , and (d) the gap at $(\pi, 0)$ for the cases of $(J_1, J_2) = (0.2, 0.8), (0.1, 0.9), (0.0, 1.0)$.

ering them failed for the cases of (J_1, J_2) (0.7, 0.3), (0.6, 0.4), (0.5, 0.5), (0.4, 0.6), (0.3, 0.7).these cases we take an alternative approach of starting from the zero-temperature results and then increase the temperature. The results are shown in Fig. 9. The variations in the specific heat and spin susceptibility are nonmonotonic. Initially, the peak in the specific heat decreases and then increases as J_2 is raised. Similarly, the magnitude of the spin susceptibility first increases and then decreases with increasing J_2 , indicating enhanced fluctuations around $(J_1, J_2) \sim (0.6, 0.4)$. In contrast, the changes in the gaps are more uniform. Both $\Delta(\pi,\pi)$ and $\Delta(\pi,0)$ decrease almost monotonically as J_2 increases. For the case of $(J_1, J_2) \sim (0.6, 0.4)$, the magnitudes of the gaps suggest a lack of significant antiferromagnetic correlations associated with the interactions J_1 and J_2 , indicating that the system is distant from the long-range ordered state. While the results seem plausible, they are not entirely convincing. Clearly, further numerical calculations that correlate with the high-temperature expansion results are necessary. Such studies are reserved for future research.

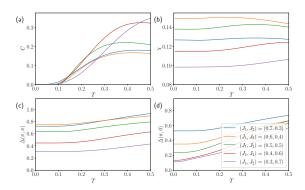


FIG. 9. (Color online) Temperature dependencies for (a) the specific heat, (b) the spin susceptibility, (c) the gap at (π, π) , and (d) the gap at $(\pi, 0)$ for the cases of $(J_1, J_2) = (0.7, 0.3), (0.6, 0.4), (0.5, 0.5), (0.4, 0.6), (0.3, 0.7).$

To obtain reliable results for the J_1 - J_2 model, there are two possible approaches. One option is to perform a three-dimensional calculation by considering a quasi-two-dimensional system. Such a calculation was carried out[30] using several decoupling parameters and incorporating input from exact diagonalization while introducing an approximate expression for the ground state energy. If we introduce one decoupling parameter, there is no need to consider inputs from other methods. Another approach involves implementing the decoupling approximation at the third-order equation of motion. These aspects remain to be explored in future research.

V. SUMMARY

To summarize, we have presented a generalized formulation of the Green's function method that can be applied to diverse antiferromagnetic Heisenberg spin systems. We have discussed the hypercubic lattice and the J_1 - J_2 model as specific applications. We have derived the spin-wave dispersion formula for the hypercubic lattice in any spatial dimension. We have shown that for d=1 and d=2, our formula yields accurate results at high temperatures, and for d=3, it predicts the transition temperature with greater precision than mean field theory, closely aligning with the quantum Monte Carlo results. For the case of the J_1 - J_2 model, we computed the correlation functions at zero temperature and spinwave dispersion. Although we have included the effect of nematic correlation, there is no signature of the nematic order. At finite temperatures, we calculate the specific heat, spin susceptibility, and gaps at characteristic wave vectors. We achieve reasonable results when the effect

of frustration is weak. However, we are unable to obtain results consistent with the high-temperature expansion when the effect of frustration is pronounced.

We note that the Green's function approach can be generalized to incorporate other interactions and higher spin values. The key features of this approach are that it does not need to assume specific correlations and enables the investigation of finite temperature and dynam-

ical properties.

Exploring higher-order approximations in the decoupling scheme is promising, and it may provide more accurate results and a better understanding of the physical behavior of the spin system. Such investigation can open up new insights into the spin system and pave the way for more accurate and comprehensive theoretical descriptions.

- B. Keimer, S. Kivelson, M. Norman, S. Uchida, and J. Zaanen, Nature 518, 179 (2015).
- [2] P. Anderson, Mater. Res. Bull. 8, 153 (1973).
- [3] L. Balents, Nature 464, 199 (2010).
- [4] L. Savary and L. Balents, Rep. Progr. Phys. 80, 016502 (2017).
- [5] Y. Zhou, K. Kanoda, and T.-K. Ng, Rev. Mod. Phys. 89, 025003 (2017).
- [6] S. Tyablikov and V. Bonch-Bruevich, Adv. Phys. 11, 317 (1962).
- [7] D. N. Zubarev, Sov. Phys. Usp. 3, 320 (1960).
- [8] J. Kondo and K. Yamaji, Progr. Theoret. Phys. 47, 807 (1972).
- [9] Y. A. Tserkovnikov, Theoret. Math. Phys. 49, 993 (1981).
- [10] H. Shimahara and S. Takada, J. Phys. Soc. Jpn. 60, 2394 (1991).
- [11] T. Xiang, Phys. Rev. B 58, 9142 (1998).
- [12] Y. Okabe and M. Kikuchi, J. Phys. Soc. Jpn. 57, 4351 (1988).
- [13] J.-K. Kim and M. Troyer, Phys. Rev. Lett. 80, 2705 (1998).
- [14] T. Morinari, J. Phys. Soc. Jpn. 87, 063707 (2018).
- [15] A. Barabanov and E. Zhasinas, Phys. Lett. A 193, 191 (1994).
- [16] A. W. Sandvik, Phys. Rev. Lett. 80, 5196 (1998).
- [17] P. Chandra and B. Doucot, Phys. Rev. B 38, 9335 (1988).
- [18] M. P. Gelfand, R. R. P. Singh, and D. A. Huse, Phys.

- Rev. B **40**, 10801 (1989).
- [19] E. Dagotto and A. Moreo, Phys. Rev. Lett. 63, 2148 (1989).
- [20] F. Figueirido, A. Karlhede, S. Kivelson, S. Sondhi, M. Rocek, and D. S. Rokhsar, Phys. Rev. B 41, 4619 (1990).
- [21] H.-C. Jiang, H. Yao, and L. Balents, Phys. Rev. B 86, 024424 (2012).
- [22] W.-J. Hu, F. Becca, A. Parola, and S. Sorella, Phys. Rev. B 88, 060402 (2013).
- [23] S.-S. Gong, W. Zhu, D. Sheng, O. I. Motrunich, and M. P. Fisher, Phys. Rev. Lett. 113, 027201 (2014).
- [24] L. Wang and A. W. Sandvik, Phys. Rev. Lett. 121, 107202 (2018).
- [25] F. Ferrari and F. Becca, Phys. Rev. B 102, 014417 (2020).
- [26] Y. Nomura and M. Imada, Phys. Rev. X 11, 031034 (2021).
- [27] O. Gauthé and F. Mila, Phys. Rev. Lett. 128, 227202 (2022).
- [28] L. Siurakshina, D. Ihle, and R. Hayn, Phys. Rev. B 64, 104406 (2001).
- [29] T. Hutak, T. Krokhmalskii, O. Derzhko, and J. Richter, Eur. Phys. J. B 95, 93 (2022).
- [30] D. Schmalfuß, R. Darradi, J. Richter, J. Schulenburg, and D. Ihle, Phys. Rev. Lett. 97, 157201 (2006).